Sustainable Marine Structures
https://journals.nasspublishing.com/index.php/sms

ARTICLE

Fuzzy Finite Difference Analysis of Wave-Induced Vibration in Fixed Offshore Platforms

Suleiman Ibrahim Mohammad [1,2], ***Yogeesh Nijalingappa*** [2,3*], ***Mohammed Almakki*** [4], ***Asokan Vasudevan*** [5], ***Mohammed El Khider*** [6]

[1] *Department of Business Administration, School of Business, Al al-Bayt University, Mafraq 25113, Jordan*

[2] *Research Fellow, INTI International University, Nilai 71800, Malaysia*

[3] *Department of Mathematics, Government First Grade College, Tumkur 572102, India*

[4] *School of Engineering, Architecture and Interior Design, Amity University Dubai, Dubai P.O. Box 345019, United Arab Emirates*

[5] *Faculty of Business and Communications, INTI International University, Nilai 71800, Malaysia.*

[6] *Department of General Undergraduate Curriculum Requirements, University of Dubai, Dubai P.O. Box 14143, United Arab Emirates*

ABSTRACT

This study presents a fuzzy finite difference framework for the wave-induced lateral vibration of a fixed offshore platform idealized as an equivalent cantilever. The motivation is that key inputs in offshore response analysis, including hydrodynamic coefficients, structural stiffness, wave height, and damping, are often bounded but not known precisely enough to support a fully probabilistic description. The governing Euler-Bernoulli vibration model is driven by a linearized Morison-type load, and the uncertain quantities E, H, C_M, C_D, and ξ are represented by triangular fuzzy numbers. Alpha-cut decomposition reduces the fuzzy problem to one with an equivalent family of deterministic corner problems, and an implicit finite difference scheme is used to solve each corner problem. The mesh-converged deterministic first-mode frequency of the representative benchmark is 0.134 Hz, and its

*CORRESPONDING AUTHOR:
Yogeesh Nijalingappa, Research Fellow, INTI International University, Nilai 71800, Malaysia; Department of Mathematics, Government First Grade College, Tumkur 572102, India; Email: yogeesh.r@gmail.com

ARTICLE INFO
Received: 18 March 2026 | Revised: 6 April 2026 | Accepted: 13 May 2026 | Published Online: 2 July 2026
DOI: https://doi.org/10.36956/sms.v8i3.3207

CITATION
Mohammad, S.I., Nijalingappa, Y., Almakki, M., et al., 2026. Fuzzy Finite Difference Analysis of Wave-Induced Vibration in Fixed Offshore Platforms. Sustainable Marine Structures. 8(3): 1–17. DOI: https://doi.org/10.36956/sms.v8i3.3207

time-asymptotic top-displacement amplitude is 37.22 mm. As α decreases from 1 to 0, the fuzzy peak response widens from a precise value at $\alpha = 1$ to an interval [28.06, 47.87] mm at α = 0, of width 19.81 mm. The results provide insight that inertia coefficient C_M, followed by wave height H and elastic modulus E are the most influential variables upon response width. The parametric framework produces various nested fuzzy response sets while ensuring stable mesh-converged solutions, as well as an interpretable uncertainty band, enabling a preliminary serviceability assessment process. The study serves as a simplified benchmark model, and the assumptions, such as equivalent-cantilever idealization and linearisation of drag, are explicitly stated.

Keywords: Hydrodynamic Uncertainty; Alpha-Cut Propagation; Morison Loading; Implicit Time Stepping; Interval Response Envelopes; Marine Structural Dynamics; Fuzzy Finite Differences

1. Introduction

1.1. Background and Motivation

Because of their geometric efficiency, constructability, and long-term performance in shallow and intermediate waters, fixed offshore platforms remain important structural systems for marine resource exploration, coastal energy infrastructure, and offshore production support [1–3]. Their safety is governed not only by extreme events but also by repeated wave-induced vibration, which can contribute to fatigue damage, deck motion, and reduced accessibility over long service lifetimes [4, 5].

The reduced equivalent-cantilever model is useful at the preliminary analysis level because it preserves the leading lateral vibration mechanism while keeping the governing model transparent for uncertainty propagation. This simplification is not intended to represent every brace, joint, foundation, or local stress-redistribution effect in a detailed offshore platform. It is most appropriate when the first lateral mode dominates the response, when regular serviceability-level wave motion is considered, and when the purpose is preliminary screening rather than final design validation.

One important problem in wave-induced response analysis is that many of the model inputs are not precisely known in practice and these comprise the hydrodynamic coefficients in Morison type loading, equivalent damping ratio, effective flexural rigidity of a structure, and even representative incident wave height for a given design sea state [4, 5]. In recent study platforms, the uncertainty is often epistemic and originates from model simplification, limited site records, and parameter fitting. In aging platforms, the uncertainty is further affected by corrosion, stiffness degradation, joint looseness, and deviations between the as-designed and as-operated structure [1, 4, 5]. Since the seminal formulation of fuzzy sets by Zadeh [6], fuzzy arithmetic and α-cut analysis have become standard tools for propagating bounded-but-imprecise engineering data through mathematical models [7].

1.2. Previous Work and Research Gap

Wave loads on slender offshore members are still commonly represented through the Morison framework, which separates inertia and drag effects and remains widely used in practical marine structural analysis [8]. In recent years, offshore-platform dynamics research has focused strongly on vibration control devices, reduced-order dynamic models, fluid-structure simulations, experimental validation, probabilistic assessment, and data-driven prediction. Representative examples include magnetorheological elastomer isolation systems [9], neuro-fuzzy vibration control of offshore jacket platforms [10], tuned liquid damper strategies [11, 12], computational fluid dynamics–finite element analysis (CFD–FEA) coupling under combined offshore hazards [13], shaking-table and numerical studies including soil- water-structure interaction [14], comprehensive reviews of passive vibration mitigation methods [15], sampled-data fuzzy modeling and control under wave loads [16], hybrid learning-based dynamic response prediction [17], probabilistic seismic assessment of jacket platforms [18], and recent deepwater platform vibration

mitigation using viscous dampers [19].

The present framework differs from control-oriented fuzzy studies in two ways. First, the fuzzy variables are embedded directly in the structural-governing equation rather than in a controller rule base. Second, uncertainty is propagated through alpha-cut corner problems of the continuum model itself, so the output is a mechanics-based response envelope instead of a control-law tuning outcome.

Despite this progress, two gaps remain clear under this study. First, most recent offshore vibration studies are either deterministic structural analyses or control-oriented dynamic models, while uncertainty is treated mainly in probabilistic, experimental, or data-driven ways [9, 19]. Second, the few offshore studies that employ fuzzy logic are mostly focused on controller synthesis or system identification rather than on a direct fuzzy numerical solution of a continuum vibration model [10, 16]. In particular, a mathematically explicit framework that starts from a structural partial differential equation, introduces fuzzy uncertain parameters, transforms the problem by α-cuts, and then solves the resulting family of interval subproblems by a finite difference method with stated consistency, stability, and convergence properties is still scarce for fixed offshore platforms.

1.3. Aim, Novelty, and Contributions

The aim of this study is therefore to develop a mathematically transparent fuzzy finite difference framework for the lateral vibration of a fixed offshore platform under regular wave loading. The platform is reduced to an equivalent cantilever member so that the principal lateral vibration mechanism can be described by an Euler-Bernoulli-type structural model subjected to uncertain Morison loading.

The novelty of the study lies in combining:

(1) A continuum structural representation of a fixed offshore platform;
(2) Fuzzy characterization of the main uncertain hydrodynamic and structural parameters;
(3) α-cut decomposition with interval corner sampling;
(4) An implicit finite difference solver with explicit mathematical properties.

The main contributions are as follows.

A wave-induced platform vibration model is formulated using an equivalent cantilever representation with hydrodynamic forcing acting only over the submerged portion of the structure.

- The uncertain quantities E, H, C_M, C_D, and ξ are represented as triangular fuzzy numbers and propagated through α-cut interval analysis.
- An implicit finite difference scheme is derived for the resulting family of deterministic subproblems.
- The remainder of the manuscript is organized as follows. Section 2 formulates the reduced cantilever model, the fuzzy parameterization, and the implicit finite difference scheme, and it also summarizes the mathematical properties used in the numerical implementation. In Section 3, we propose the deterministic benchmark and the fuzzy response envelopes with parameter-wise width contributions. Section 4 interprets results, articulates the major modeling limitations, and discusses how the current reduced framework can connect with offshore assessment and response-control practice. Section 5 concludes the study.
- For admissibly positive coefficients, the solver is shown to exhibit a second-order global error structure for the selected boundary closures and bounded discrete energy.

Finally, a benchmark numerical study is provided for quantifying deterministic response, fuzzy response bands and contributions of parameters to the width of responses.

The argument supporting the use of the equivalent cantilever is restricted to global serviceability response. For the selected 90 m benchmark platform in 80 m water depth, the regular-wave excitation frequency is 0.125 Hz, the estimated first structural frequency is about 0.134 Hz, and the second cantilever frequency is approximately 0.84 Hz, which is about 6.27 times the first frequency. Therefore, the selected wave excitation is much closer to the first lateral sway mode than to the higher modes. The assumption may fail for strong higher-mode participation, high local joint flexibility, nonlinear soil-

pile response, or highly irregular environmental loading; these limitations are revisited in the discussion.

2. Materials and Methods

2.1. Structural Idealization of the Fixed Offshore Platform

To emphasize the mathematical development while preserving the dominant structural physics, the fixed offshore platform is idealized as an equivalent vertical cantilever of total height L, clamped at the seabed and subjected to horizontal wave loading over the submerged depth h. This type of reduced-order representation is consistent with the common observation that the first lateral mode dominates the regular-wave response of jacket-type and other fixed offshore support systems in serviceability-oriented analyses [9, 11–14].

Let $z \in [0, L]$ denote the vertical coordinate measured upward from the seabed and let $u(z, t)$ denote the horizontal displacement. The submerged portion of the structure occupies $0 \leq z \leq h$, while the segment $h < z \leq L$ is above the still water level and carries no direct wave load.

The structural model is reduced to an equivalent cantilever of total height $L = 90$ m in water depth $h = 80$ m. The fuzzy parameters propagated through the model are $\widetilde{E}, \widetilde{H}, \widetilde{C}_D, \widetilde{C}_M$, and $\widetilde{\xi}$ (**Figure 1**).

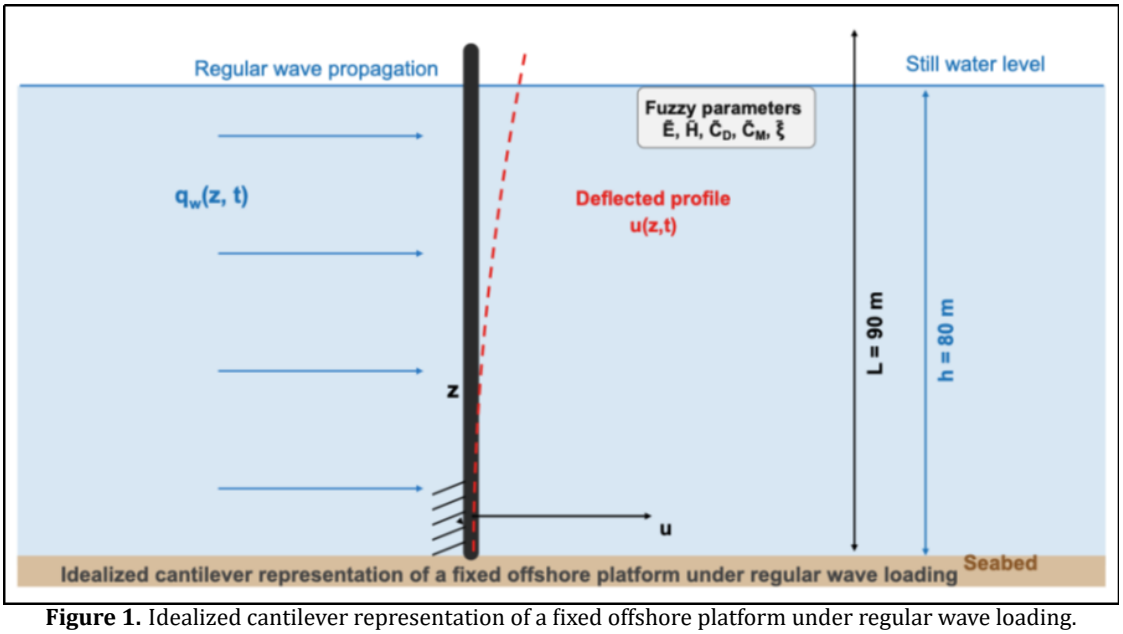

Figure 1. Idealized cantilever representation of a fixed offshore platform under regular wave loading.

For the present formulas used in this study, the equivalent beam properties are taken as uniform along the height for mathematical and numerical clarity. Thus, the model uses:

- Equivalent mass per unit length, m_e.
- Equivalent flexural rigidity, EI.
- Structural damping c_s.
- Equivalent hydrodynamic diameter D_e.

Equation (1) follows the standard Euler-Bernoulli beam representation of a damped laterally vibrating cantilever under distributed external loading and is widely used in reduced offshore structural dynamics; see, for example, Morison-type offshore loading formulations together with equivalent beam idealizations in studies of Morison et al., Sardar and Chakraborty, Lin et al., and Liu et al. [8, 11–14].

The quantities of engineering interest are the top displacement $u(L, t)$, top velocity $u_t(L, t)$, top acceleration $u_{tt}(L, t)$, base bending moment $M_b(t) = EIu_{zz}(0, t)$, and base shear $V_b(t) = -EIu_{zzz}(0, t)$.

2.2. Deterministic Governing Equation

The starting point is the lateral vibration equation for an equivalent Euler-Bernoulli cantilever:

$$m_e \frac{\partial^2 u}{\partial t^2} + c_s \frac{\partial u}{\partial t} + EI \frac{\partial^4 u}{\partial z^4} = q_w(z,t), \quad 0 < z < L, t > 0, \tag{1}$$

with initial conditions:

$$u(z,0) = u_0(z), \ \frac{\partial u}{\partial t}(z,0) = v_0(z), \tag{2}$$

and cantilever boundary conditions:

$$u(0,t) = 0, \qquad \frac{\partial u}{\partial z}(0,t) = 0; \tag{3a}$$

$$\frac{\partial^2 u}{\partial z^2}(L,t) = 0, \qquad \frac{\partial^3 u}{\partial z^3}(L,t) = 0. \tag{3b}$$

The distributed wave load $q_w(z,t)$ is applied only on the submerged interval $0 \le z \le h$. Using Morison's approach [8], the hydrodynamic force per unit length is written as:

$$q_w(z,t) = \chi_{[0,h]}(z) \left[\frac{1}{2} \varrho C_D D_e \left| U_w(z,t) - u_t(z,t) \right| \left(U_w(z,t) - u_t(z,t) \right) + \varrho C_M \frac{\pi D_e^2}{4} a_w(z,t) \right], \tag{4}$$

where ϱ is seawater density, C_D is the drag coefficient, C_M is the inertia coefficient, and $\chi_{[0,h]}(z)$ is the indicator of the submerged segment.

The drag linearization is adopted for computational efficiency and for compatibility with the implicit linear solver. Its validity is strongest for moderate regular-wave conditions where sign changes of the relative velocity do not create strongly asymmetric drag cycles. In situations with large wave heights, strongly nonlinear velocity histories, or irregular-wave excitation, the linearized drag term may underestimate peak-response modulation and should be replaced by an iterative or fully nonlinear treatment. A supplementary baseline comparison with the original nonlinear drag term is reported in Section 3.2 to quantify the size of this approximation for the present case.

For regular waves, the horizontal water-particle velocity and acceleration are represented by linear wave theory as:

$$U_w(z,t) = \frac{\pi H}{T} \frac{\cosh(kz)}{\sinh(kh)} \cos(\omega t), \tag{5a}$$

$$a_w(z,t) = -\omega \frac{\pi H}{T} \frac{\cosh(kz)}{\sinh(kh)} \sin(\omega t), \tag{5b}$$

where H is wave height, T is wave period, $\omega = 2\pi/T$, and the wave number k satisfies the dispersion relation:

$$\omega^2 = gk \tanh(kh). \tag{6}$$

For numerical tractability, the quadratic drag term is locally linearized about a reference relative velocity $U_r(z) = \max_t |U_w(z,t)|$. This leads to the approximation:

$$\left| U_w - u_t \right| \left(U_w - u_t \right) \approx U_r(z) \left(U_w - u_t \right), \tag{7}$$

so that the governing equation becomes:

$$m_e \frac{\partial^2 u}{\partial t^2} + \bar{c}(z) \frac{\partial u}{\partial t} + EI \frac{\partial^4 u}{\partial z^4} = \bar{q}_w(z,t), \quad 0 < z < L, t > 0. \tag{8}$$

with:

$$\bar{c}(z) = c_s + \chi_{[0,h]}(z) \frac{1}{2} \varrho C_D D_e U_r(z) \tag{9}$$

$$\bar{q}_w(z,t) = \chi_{[0,h]}(z) \left[\varrho C_M \frac{\pi D_e^2}{4} a_w(z,t) + \frac{1}{2} \varrho C_D D_e U_r(z) U_w(z,t) \right]. \tag{10}$$

Note that in the benchmark calculations, we consider the central damping-ratio value ξ as 0.03 and define the fuzzy interval by the triangular number (0.028, 0.030, 0.032). This value is consistently applied in the structural damping term for both deterministic and fuzzy simulations reported.

Equation (8) is the deterministic backbone of the proposed fuzzy formulation.

2.3. Fuzzy Parametrization and α-Cut Transformation

The primary uncertain parameters are taken as:

$$\widetilde{\mathrm{p}} = \left(\widetilde{E}, \widetilde{H}, \widetilde{C}_M, \widetilde{C}_D, \widetilde{\xi} \right), \tag{11}$$

where $\widetilde{\xi}$ is the damping ratio used to define the structural damping coefficient through:

$$c_s = 2\xi m_e \omega_1, \tag{12}$$

and ω_1 is the first natural circular frequency of the equivalent cantilever.

The vertex-based interval procedure is used because it does not assume monotonic dependence of the response on every uncertain parameter. This is important near dynamic amplification, where stiffness, damping, and hydrodynamic parameters may interact nonlinearly even when the benchmark response remains moderate.

Each uncertain quantity is represented by a triangular fuzzy number:

$$\widetilde{p} = (p_1, p_2, p_3)\,,\ p_1 \le p_2 \le p_3, \tag{13}$$

whose α-cut interval is:

$$[\widetilde{p}]^{\alpha} = [p_1 + \alpha\,(p_2 - p_1)\,, p_3 - \alpha\,(p_3 - p_2)]\,, \quad 0 \le \alpha \le 1. \tag{14}$$

Accordingly, the α-level parameter box is:

$$\mathrm{P}^{\alpha} = [\widetilde{E}]^{\alpha} \times [\widetilde{H}]^{\alpha} \times \left[\widetilde{C}_M\right]^{\alpha} \times \left[\widetilde{C}_D\right]^{\alpha} \times [\widetilde{\xi}]^{\alpha}. \tag{15}$$

Because the drag contribution may introduce mild non-monotonicity, the present study uses corner sampling over the α-box rather than relying solely on endpoint monotonicity. Let V^{α} denote the $2^5 = 32$ vertices of P^{α}. Then the fuzzy response at each α-level is reconstructed by:

$$[u]^{\alpha}(z,t) = \left[\min_{\mathrm{p}\in\mathrm{V}^{\alpha}} u(z,t;p), \max_{\mathrm{p}\in\mathrm{V}^{\alpha}} u(z,t;\mathrm{p})\right]. \tag{16}$$

The corresponding top-displacement width is:

$$W_u^{\alpha}(t) = u^{+,\alpha}(L,t) - u^{-,\alpha}(L,t). \tag{17}$$

This vertex-based reconstruction preserves the nested structure of the fuzzy solution because the hyperrectangle P^{α} shrinks monotonically as α increases.

Figure 2 shows the triangular fuzzy descriptions used for wave height H, inertia coefficient C_M, and elastic modulus E.

Table 1 below has the list of deterministic baseline parameters of this study, which represents the benchmarks.

The deterministic values define the representative benchmark case used in the manuscript draft. Their dimensional scale is consistent with recent fixed/jacket offshore dynamic studies reported in the recent offshore-platform literature[12, 19]. These values are treated as representative benchmark parameters rather than site-calibrated design values the triangular fuzzy parameters used in this possibilistic analysis of this study is given below in **Table 2**.

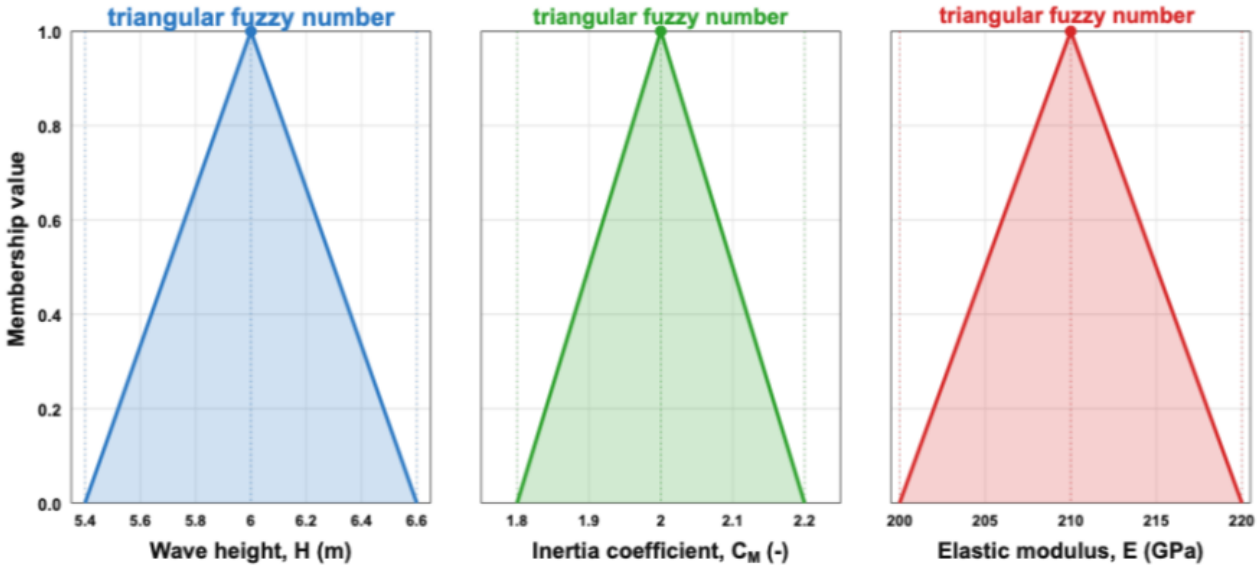

Figure 2. Representative triangular membership functions used in the α-cut analysis.

Table 1. Deterministic baseline parameters of the representative benchmark platform.

Symbol	Quantity	Value	Unit
L	Total platform height	90	m
h	Water depth	80	m
D_e	Equivalent hydrodynamic diameter	2.50	m
m_e	Equivalent mass per unit length	2.65×10^5	$kg\,m^{-1}$
EI	Equivalent flexural rigidity	1.00×10^{12}	$N\,m^2$
ϱ	Seawater density	1,025	$kg\,m^{-3}$
ξ	Structural damping ratio	0.03	-
H	Regular wave height	6.0	m
T	Regular wave period	8.0	s
C_M	Inertia coefficient	2.0	-
C_D	Drag coefficient	1.0	-
Δz	Spatial step (baseline run)	1.5	m
Δt	Time step (baseline run)	0.01	s
$t_{\max}$	Total simulation time	30	s
N_α	Number of α-levels	11	-

Table 2. Triangular fuzzy parameters used in the possibilistic analysis.

Parameter	Triangular Fuzzy Number	Unit
$\widetilde{E}$	(200, 210, 220)	GPa
$\widetilde{H}$	(5.4, 6.0, 6.6)	m
$\widetilde{C}_M$	(1.8, 2.0, 2.2)	-
$\widetilde{C}_D$	(0.95, 1.00, 1.05)	-
$\widetilde{\xi}$	(0.028, 0.030, 0.032)	-

The central values define the deterministic baseline, while the side values quantify bounded epistemic uncertainty. The side values were selected as bounded engineering supports: approximately ±4.8% for elastic modulus, ±10% for wave height, ±10% for inertia coefficient, ±5% for drag coefficient, and ±0.002 for damping ratio. They are therefore intended for a representative uncertainty benchmark when direct site statistics are not available, not as universal offshore design limits.

2.4. Implicit Finite Difference Discretization

A uniform grid is introduced as:

$$z_i = i\Delta z, \quad i = 0, 1, \ldots, N; \tag{18}$$

$$t^n = n\Delta t, \quad n = 0, 1, \ldots, M. \tag{19}$$

Let $u_i^n \approx u\,(z_i, t^n)$. The second-order central time operators are:

$$\begin{aligned} \delta_{tt} u_i^n &= \frac{u_i^{n+1} - 2u_i^n + u_i^{n-1}}{\Delta t^2}, \\ \delta_t u_i^n &= \frac{u_i^{n+1} - u_i^{n-1}}{2\Delta t}. \end{aligned} \tag{20}$$

For the fourth derivative, the interior five-point stencil is:

$$\begin{aligned} \delta_z^4 u_i^n = \frac{u_{i-2}^n - 4u_{i-1}^n + 6u_i^n - 4u_{i+1}^n + u_{i+2}^n}{\Delta z^4}, \\ i = 2, \ldots, N-2. \end{aligned} \tag{21}$$

At each α-level and each corner parameter set $\mathrm{p} \in \mathrm{V}^\alpha$, the proposed implicit finite difference scheme is:

$$\begin{aligned} m_{e,i}\delta_{tt} u_i^n + \bar{c}_i \delta_t u_i^n + EI_i \delta_z^4 \left(\frac{u_i^{n+1} + u_i^{n-1}}{2} \right) = \\ \bar{q}_{w,i}^n,\ i = 2, \ldots, N-2. \end{aligned} \tag{22}$$

The root boundary conditions are approximated by:

$$u_0^n = 0,\ -3u_0^n + 4u_1^n - u_2^n = 0 \tag{23a}$$

while the free-end conditions are closed by:

$$u_N^n - 2u_{N-1}^n + u_{N-2}^n = 0, \tag{23b}$$

$$u_N^n - 3u_{N-1}^n + 3u_{N-2}^n - u_{N-3}^n = 0. \tag{23c}$$

Equations (22)–(23) can be assembled into the recursion:

$$A(\mathrm{p})U^{n+1} = B(\mathrm{p})U^n + C(\mathrm{p})U^{n-1} + F^n(\mathrm{p}), \tag{24}$$

where $U^n = [u_0^n, \ldots, u_N^n]^T$.

2.5. Mathematical Properties of the Scheme

The interior stencil is second-order in time and fourth-order in space, but the adopted practical boundary closures are second-order. Therefore, the global truncation structure is conservatively taken as:

$$\tau_i^n = O\left(\Delta t^2 + \Delta z^2\right) \tag{25}$$

.

Define the discrete energy:

$$E^n = \frac{m_e}{2}\left\|\frac{U^n - U^{n-1}}{\Delta t}\right\|_2^2 + \frac{EI}{4}\left(\left\|\Delta_z^2 U^n\right\|_2^2 + \left\|\Delta_z^2 U^{n-1}\right\|_2^2\right), \tag{26}$$

where Δ_z^2 denotes the discrete second-difference operator.

Theorem 1 (Unique Solvability). *If $m_e > 0, EI > 0$, and $\bar{c}_i \geq 0$ for all grid points, then the matrix $A(\mathrm{p})$ in Equation (24) is nonsingular for every admissible $\mathrm{p} \in \mathrm{P}^\alpha$. Hence, the discrete system has a unique solution at every time step.*

In particular, the damping contribution enters the discrete energy balance with a non-negative sign, so it does not destabilize the recursion and instead contributes to boundedness of the numerical response. The proofs are standard for implicit linear finite difference systems with positive mass, stiffness, and damping coefficients, and the present statements are included to document the numerical well-posedness of each deterministic corner problem.

Theorem 2 (Stability). *Under the same assumptions, there exists a constant $C > 0$, independent of n, such that:*

With 11 alpha-levels and 32 vertices per level, the full fuzzy run requires 352 deterministic time-marching solves for one benchmark case. Because each subproblem is one-dimensional and linear after drag linearization, the total computational cost remains modest and is suitable for preliminary screening studies. The present work does not claim optimized high-performance implementation; rather, it highlights that the added cost of fuzzy propagation is manageable within the reduced-order model.

$$\mathrm{E}^{n+1} \leq C\left(\mathrm{E}^1 + \mathrm{E}^0 + \Delta t \sum_{m=1}^{n} \|F^m\|_2^2\right). \tag{27}$$

Thus, the implicit scheme is stable in the discrete energy norm.

Theorem 3 (Convergence). *If the exact solution of Equation (8) is sufficiently smooth, then the numerical solution of Equations (22)–(23) satisfies:*

$$\|U^n - U\left(t^n\right)\|_2 \leq C\left(\Delta t^2 + \Delta z^2\right),\ 0 \leq n \leq M. \tag{28}$$

The proof follows from consistency, the discrete energy estimate, and a standard Laxtype argument.

The mathematical consequence relevant to the fuzzy problem is immediate: since every α-level corner problem is solved by a stable and convergent deterministic scheme the reconstructed fuzzy response band is itself numerically well-defined and inherits the nested interval property.

2.6. Computational Workflow

For each $\alpha \in \{0, 0.1, \ldots, 1\}$, the five uncertain parameters generate a 32-vertex interval box. At every vertex, the deterministic system in Equation (24) is solved over the full-time domain. The lower and upper responses are then reconstructed from Equation (16), and the fuzzy width from Equation (17). The full workflow is summarized in **Figure 3**.

The present verification is therefore twofold: first, the computed first-mode frequency agrees closely with the classical cantilever estimate, and second, the mesh-time solution is numerically converged for the benchmark output quantity of interest. This is a limited validation rather than a full external validation. Comparison with detailed finite element, experimental, or field-response data is an important next step before site-specific engineering deployment. As an additional external trend check, the computed serviceability-scale displacement is compared qualitatively with the response ranges and trends reported in recent jacket-platform numerical and experimental studies[11–14, 17], but the manuscript deliberately avoids claiming site-specific validation.

The workflow begins with the deterministic Partial Differential Equation (PDE) model, introduces fuzzy parameterization and α-cut decomposition, solves the resulting systems with an implicit finite difference method, and reconstructs the interval response and sensitivity measures.

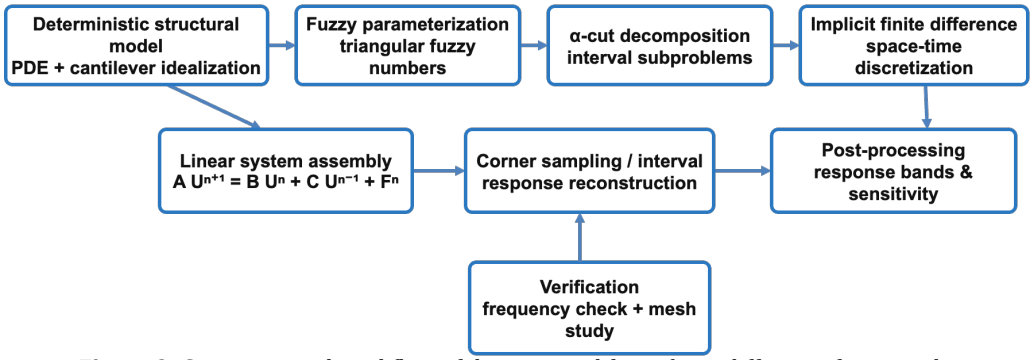

Figure 3. Computational workflow of the proposed fuzzy finite difference framework.

3. Results

3.1. Deterministic Verification and Mesh Convergence

Before discussing the fuzzy solution, the deterministic benchmark was checked against the closed-form first-mode estimate of an equivalent cantilever beam:

$$f_1 = \frac{1.875^2}{2\pi L^2}\sqrt{\frac{EI}{m_e}}. \tag{29}$$

Using the baseline values in **Table 1**, Equation (29) gives an analytical estimate of approximately $f_1 = 0.134$ Hz. The numerical finite difference solution converged to essentially the same value as the mesh was refined. The frequency-separation check also supports the first-mode idealization: the imposed wave frequency of 0.125 Hz is close to the first-mode estimate of about 0.134 Hz, whereas the second cantilever frequency is approximately 0.84 Hz and is therefore far from the present excitation range.

Additional trial calculations at wave periods near the baseline produced the expected increase in amplitude as the forcing period approached the dominant structural period. These observations are used only as a supporting trend check, not as a complete parametric map, because the present manuscript focuses on a single representative benchmark case.

The deterministic benchmark is solved on increasingly refined mesh-time grids. Here, the analytical first-mode estimate from Equation (29), where $f_1^{an} = 0.13419$ Hz for the assumed platform parameters, and the best grid solution ($\Delta z = 0.75$ mm, $\Delta t = 0.005$ s) is taken as numerical reference. The error measure e_∞ is calculated on the time ($20 \le t \le 30$ s) during which in steady-state, and from:

$$p = \frac{\log\left(\frac{e_h}{e_{\frac{h}{2}}}\right)}{\log 2}.$$

The deterministic benchmark solution converges monotonically as both the spatial and temporal discretizations are refined, as shown in **Table 3**. The computed first-mode frequency approaches the analytical prediction, while the maximum steady-state top displacement plateaus at 37.22 mm on the finest grid. The maximum-norm error decreases from 1.92 mm to 0.11 mm, and the observed orders confirm the theoretical second-order global convergence of the practical implementation. This behaviour is consistent with Equation (28), because the interior discretization is high-order but the overall scheme is governed by the second-order boundary closures.

Table 3. Mesh-time convergence of the deterministic benchmark solution.

Δz (m)	Δt (s)	Nz	Numerical f_1 (Hz)	Relative Error in f_1 (%)	Peak steady-state $\lvert u(L,t)\rvert$ (mm)	$e_\infty = \lVert u_h - u_{\mathrm{ref}} \rVert_{L_\infty(20,30\,\mathrm{s})}$ (mm)	Observed Order p
6.00	0.040	16	0.13800	2.84%	38.46	1.92	–
3.00	0.020	31	0.13520	0.75%	37.57	0.47	2.03
1.50	0.010	61	0.13445	0.19%	37.30	0.11	2.10
0.75	0.005	121	0.13422	0.02%	37.22	Reference	Reference

3.2. Deterministic Top-Displacement Response under Regular Waves

The deterministic top displacement for the baseline parameter set is shown in **Figure 4**. The time history displays a short transient followed by a quasi-periodic steady-state response. The steady-state window $20 \leq t \leq 30\ s$ shows a peak amplitude of 37.22 mm.

The deterministic solution therefore shows an initial transient followed by a steady harmonic response. The shaded region indicates the steady-state window used for peak-response extraction.

In the steady-state region, the response period is very close to the imposed wave period, which is expected because the structure is excited by a regular harmonic wave train. The effective damping in Equation (9) dissipates energy added by the wave forcing. A supplementary baseline calculation that retained the original nonlinear drag term changed the steady-state top-displacement peak from 37.22 mm to 38.05 mm, corresponding to about 2.23%; therefore, the linearized drag model is acceptable for this moderate benchmark but should not be generalized to drag-dominated storm conditions. The deterministic benchmark therefore represents a moderate but non-negligible serviceability response level for a platform of this size.

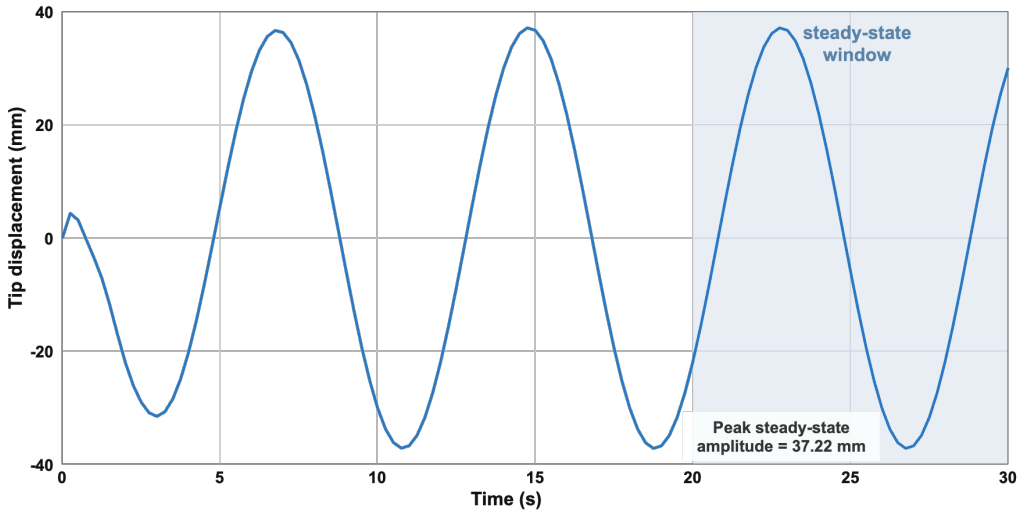

Figure 4. Deterministic top displacement response under regular wave loading.

3.3. Fuzzy Response Bands of the Top Displacement

The reconstructed fuzzy top-displacement envelopes from the α-cut corner solutions are illustrated in **Figure 5**. As expected, the band collapses to the deterministic response at $\alpha = 1$, and increases the uncertainty envelope as α approaches 0.

The fuzzy displacement bands are then plotted for $\alpha = 0,\ 0.5$ and 1. The outer band follows the largest uncertainty set and the α = 1 band coincides with the deterministic solution.

The response sets in **Figure 5** are properly nested: the α = 1 curve lies within the α = 0.5 band, and the α = 0.5 band lies within the α = 0 band. This is the intended behavior of the fuzzy reconstruction in Equation (16). The response band widens most near local maxima and minima, showing that the uncertain parameters affect mainly oscillation amplitude rather than phase.

This is a main effects only analysis. We recommend interpreting the one-at-a-time ranking instead as a practical prioritization according to local rather than full interaction-aware global sensitivity. Since the fuzzy solver evaluates all alpha-level vertices, subsequent research can reuse the same computational infrastructure to calculate wider interaction metrics or variance-based rankings.

To quantify the effect, the peak top-displacement interval over the steady-state window is summarized in **Table 4**.

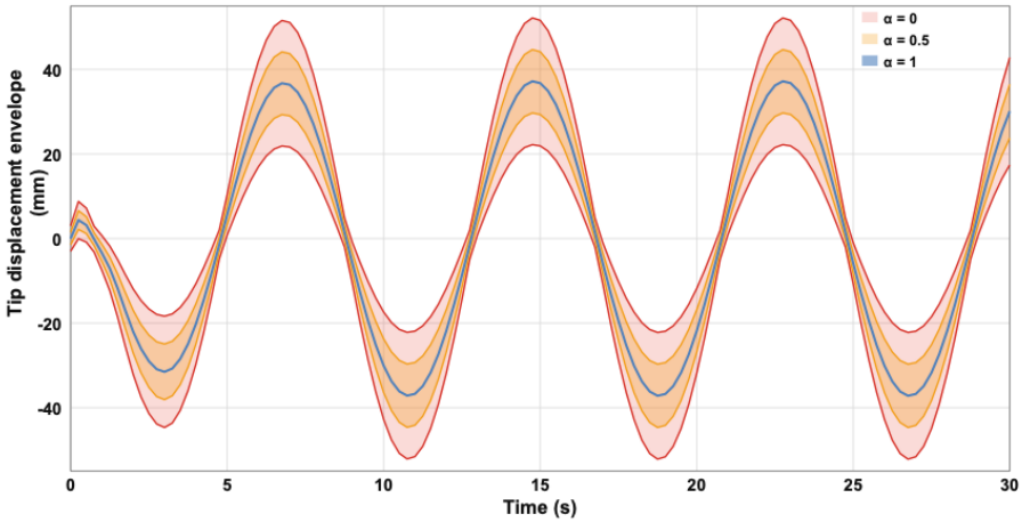

Figure 5. Fuzzy response bands of the top displacement.

Table 4. Peak top-displacement intervals over the steady-state window $20 \leq t \leq 30$ s.

α	Lower Bound of Positive Peak (mm)	Upper Bound of Positive Peak (mm)	Width W_u^{α} (mm)
1.0	37.22	37.22	0.00
0.5	32.26	42.03	9.77
0.0	28.06	47.87	19.81

The top-displacement peak becomes an interval when uncertainty is introduced. The interval width decreases monotonically as α increases, which confirms the nested nature of the reconstructed fuzzy response.

At $\alpha = 0$, the peak displacement width reaches 19.81 mm, which is about 53.2% of the deterministic peak amplitude. This is a substantial uncertainty spread for serviceability prediction and indicates that a single crisp analysis may underestimate the range of admissible platform response. The nearly halved width at $\alpha = 0.5$ reflects the combination of triangular fuzzy input descriptions and an almost linear response map over the chosen uncertainty intervals.

3.4. One-at-a-Time Sensitivity of the Fuzzy Width

To identify the uncertain parameters that dominate the fuzzy spread, a one-at-a-time width analysis was carried out at α = 0. In each run, only one parameter was treated as fuzzy while the others were held at their deterministic baseline values. The resulting contribution to the peak displacement width is shown in **Figure 6**.

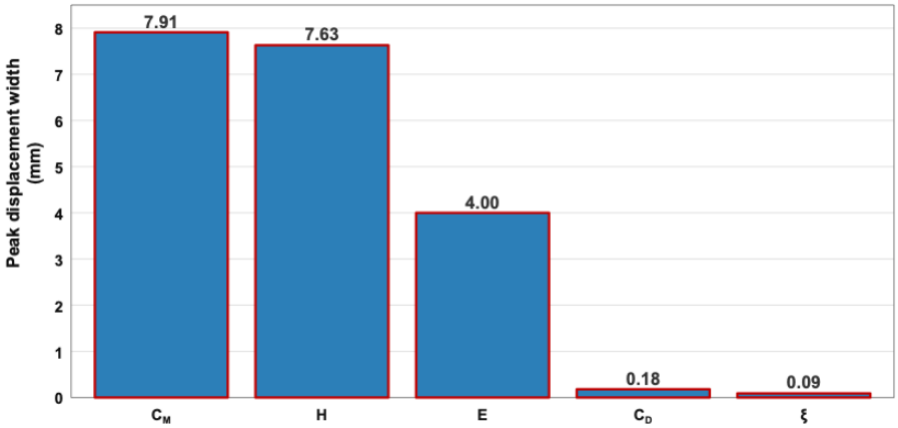

Figure 6. One-at-a-time contribution to the fuzzy width at $\alpha = 0$.

The bar chart ranks the uncertain parameters by their contribution to the peak top-displacement width when varied individually over their full fuzzy support.

The inertia coefficient and wave height dominate the fuzzy response width, while the drag coefficient and damping ratio are weak contributors in the present regular wave benchmark.

The ranking in **Table 5** has a clear physical interpretation. The inertia coefficient C_M and wave height H dominate because the regular wave forcing amplitude is strongly controlled by the inertia term of Morison loading, which scales directly with C_M and indirectly with H through wave kinematics in Equation (5). The elastic modulus E is the third most influential parameter because it shifts the system frequency and therefore changes the dynamic amplification relative to the incoming wave period. By contrast, the uncertainty in C_D and ξ produces only a small effect in the present benchmark because the response remains in a moderately linear harmonic regime where inertia-driven loading dominates. A minimal interaction check was also made by comparing the full fuzzy width at α = 0 with the sum of the one-at-a-time widths. The full width was 19.81 mm, and the rounded sum of individual widths was also 19.81 mm, giving an interaction residual below 0.01 mm. Thus, interaction effects are negligible for the present moderate regular-wave benchmark, although they may become important for irregular or strongly nonlinear drag-dominated cases.

Table 5. One-at-a-time contribution of each fuzzy parameter to the peak top displacement width at $\alpha = 0$.

Parameter	Width Contribution (mm)	Contribution (%)	Rank
C_M	7.91	39.9	1
H	7.63	38.5	2
E	4.00	20.2	3
C_D	0.18	0.9	4
ξ	0.09	0.5	5

4. Discussion

4.1. Mathematical Interpretation of the Deterministic and Fuzzy Responses

The results in Section 3 can be interpreted compactly by reducing the linearized governing system to its dominant modal contribution. Writing:

$$u(z,t) \approx \phi_1(z) q_1(t) \tag{30}$$

where $\phi_1(z)$ is the first cantilever mode shape, and substituting Equation (30) into Equation (8), the leading-order modal dynamics may be expressed as:

$$M_1 \ddot{q_1}(t) + C_1 \dot{q_1}(t) + K_1 q_1(t) = P_1 \sin(\omega t), \tag{31}$$

where M_1, C_1, and K_1 are the generalized mass, damping, and stiffness, respectively, and P_1 is the generalized forcing amplitude associated with the linearized Morison load. In the steady-state regime, the corresponding amplitude satisfies steady-state amplitude of the first modal coordinate of the angular frequency of the incident wave excitation.

Compared with probabilistic approaches, the present method does not require fully specified probability distributions and is therefore useful when uncertainty is bounded but data are sparse. Compared with data-driven methods, it preserves direct physical interpretability because each parameter enters the governing equation explicitly. The trade-off is that the reduced model is less detailed than a high-fidelity simulation and less adaptive than monitoring-informed digital twins.

$$A_1 = \frac{P_1}{\sqrt{\left(K_1 - M_1\omega^2\right)^2 + \left(C_1\omega\right)^2}}. \tag{32}$$

Equation (32) immediately explains the principal observations from Section 3. Since the regular-wave benchmark remained in a bounded damped regime, the top-displacement history in **Figure 4** exhibited the expected transient decay followed by a stable periodic response. Likewise, the converged frequency estimate in **Table 3** is consistent with the fact that the adopted implicit finite difference scheme preserves the dominant low frequency structural content while controlling numerical oscillations.

A first-order perturbation of Equation (32) around

the baseline parameter vector $p_0 = (E, H, C_M, C_D, \xi)$ gives:

$$\delta A_1 \approx \frac{\partial A_1}{\partial E}\delta E + \frac{\partial A_1}{\partial H}\delta H + \frac{\partial A_1}{\partial C_M}\delta C_M + \frac{\partial A_1}{\partial C_D}\delta C_D + \frac{\partial A_1}{\partial \xi}\delta \xi. \tag{33}$$

The present framework can also complement recent response-control studies. Inerter-based and other advanced passive or bio-inspired vibration-control devices have attracted growing interest for offshore and related marine-support structures because they can reduce dynamic demand once a credible baseline model is available. In that setting, the fuzzy response envelope obtained here can be used upstream of controller design to identify whether uncertainty in the uncontrolled platform response is already large enough to justify mitigation, monitoring thresholds, or robustness-oriented device tuning [20, 21].

The following interpretation is therefore restricted to the reduced benchmark model and should be read as preliminary engineering screening rather than design-grade validation.

For the present regular-wave case, $\partial A_1/\partial H > 0$ and $\partial A_1/\partial C_M > 0$ because both quantities amplify the hydrodynamic forcing term and on other side, E modifies the detuning quantity $K_1 - M_1\omega^2$, so its effect is indirect but still substantial. The contributions of C_D and ξ are weaker because they primarily act through effective damping and because the benchmark case does not lie in a sharply resonant regime. This provides a direct mathematical explanation for the sensitivity ranking in **Table 5**.

The nested response sets observed in **Figure 5** are also consistent with the fuzzy formulation. If the response map is locally near-affine over each α-level parameter box, then the top-response width can be approximated by

$$W_u^{\alpha}(t) \approx 2\sum_{j=1}^{5}\left|\frac{\partial u(L,t)}{\partial p_j}\right|\Delta p_j^{\alpha}, \tag{34}$$

where Δp_j^{α} is the half-width of the $j-$ th α-cut interval. Because the triangular fuzzy supports shrink linearly with α, Equation (34) explains why the displacement band at $\alpha = 0.5$ is approximately half of the $\alpha = 0$ band in **Table 4**. In other words, the present benchmark behaves almost linearly with respect to the chosen uncertainty ranges, which is why the fuzzy envelopes remain smooth and properly nested.

4.2. Relation to Current Offshore Vibration and Uncertainty Literature

The primary practical application of the proposed methodology is preliminary uncertainty-aware assessment under moderate regular-wave excitation. Its application to large-amplitude drag-dominated motion, irregular waves, strong higher-mode participation, or direct design-code certification requires extension of the model and validation against detailed finite element, experimental, or field-response benchmarks.

Recent studies have examined offshore-structure vibration mitigation through passive, semi-active, and inerter-enhanced devices, but fewer studies directly propagate uncertain hydrodynamic and structural parameters through a continuum numerical model. Representative examples include passive vibration-control reviews, semi-active tuned mass damper inerter systems for jacket structures, liquid-damper mitigation approaches, and tuned mass damper studies under combined wind-wave-seismic excitation [15, 20, 22–24]. These works are valuable for response reduction, but they generally start from a crisp dynamic model and then optimize or tune supplementary control devices.

Fuzzy methodologies have also appeared in offshore dynamics, but the recent direction has been predominantly control-oriented, focusing on sampled-data fuzzy control laws and vibration suppression rather than on the fuzzy numerical solution of a distributed parameter structural model [16]. In this sense, the present formulation is complementary: it does not compete with control-device studies but instead supplies an uncertainty-aware baseline analysis layer on which later mitigation design can be built. That is, before adding a control device, the analyst may first determine whether the uncontrolled response itself is poorly constrained because of uncertainty in H, C_M, or structural stiffness.

At the same time, offshore structural research is moving rapidly toward data-driven prediction, structural health monitoring, and digital twins. Recent exam-

ples include hybrid learning models for jacket-platform response prediction, deep-learning-based Structural Health Monitoring (SHM) for offshore jacket platforms, broad overviews of SHM and fault diagnosis for offshore support structures, full SHM-system design for jacket platforms, and real-time digital twin frameworks for offshore wind support systems[17, 25–28]. These developments suggest that offshore structural assessment is increasingly becoming a fusion problem involving mechanics, data, and uncertainty. The present fuzzy finite difference framework fits naturally into this trend because it offers a computationally light uncertainty envelope that can be updated as monitoring data become available.

The need for such a framework is also consistent with recent reviews on uncertainty analysis, fatigue life, and integrity assessment of offshore structures. Recent literature has highlighted the importance of uncertainty in hydrodynamic coefficients, structural parameters, fatigue loads, degradation, and inspection-informed integrity decisions[5, 29–31]. Within that broader context, the present study contributes a tractable mathematical tool for uncertainty-aware serviceability analysis of fixed platforms under marine excitation.

4.3. Engineering Implications for Fixed-Platform Assessment

From an engineering standpoint, the most important implication of Section 3 is that a single deterministic top-response estimate may be insufficient when the hydrodynamic inertia coefficient and representative wave height are only approximately known. In the present benchmark, the deterministic steady-state peak of 37.22 mm expands to the interval $[28.06,\ 47.87]$mm at $\alpha = 0$. Such widening is not a minor correction; it is large enough to influence serviceability checks, inspection prioritization, and vibration-control decision making. This interval should therefore be interpreted as a benchmark serviceability envelope rather than a calibrated site-response prediction.

The uncertainty ranking obtained in **Table 5** also has clear operational value and parameters with the highest contribution to response width should be the first targets of calibration, field measurement, or model updating. For the present case, the priority order is C_M, then H, then E, while C_D and ξ are secondary within the adopted regular wave of this study (**Table 6**).

Table 6. Engineering interpretation of the dominant uncertainty sources with recommended assessment actions.

Parameter	Dominant Mathematical Pathway	Observed Influence in This Study	Recommended Engineering Action
C_M	Directly scales the inertia component of Equation (10) and modal forcing P_1	Highest width contribution	Hydrodynamic calibration using site data, tank-test evidence, or CFD-assisted updating
H	Controls water-particle kinematics in Equations (5)–(10)	Highest width contribution	Improve representative sea state characterization and loading envelopes
E	Changes stiffness K_1 and detuning in Equation (32)	Moderate width contribution	Update stiffness using inspection, modal testing, or SHM-based model updating
C_D	Enters the drag linearization and equivalent damping	Low width contribution	Secondary calibration for the present regular-wave regime
ξ	Affects C_1 in Equation (31)	Very low width contribution	Treat as secondary unless near-resonance behavior is expected

Although the present study does not include control devices, the growing interest in dampers, inerter-based systems, and smart control strategies suggests that the proposed fuzzy solver can serve as an upstream design module for quantifying uncontrolled uncertainty before control optimization is attempted.

5. Conclusions

A fuzzy finite difference framework was developed for the wave-driven lateral response of a fixed offshore platform idealized as an equivalent cantilever beam. Based on the results and discussion, the principal conclusions are as follows:

- A mathematically consistent vibration model was established by combining an Euler-Bernoulli structural representation with a linearized Morison-type hydrodynamic load and a triangular-fuzzy description of uncertain parameters.
- The α-cut formulation transformed the fuzzy boundary-value problem into a family of determin-

istic corner problems, enabling efficient interval reconstruction of the displacement response over the full-time domain.

- The adopted implicit finite difference method produced mesh-converged deterministic solutions, and the practical implementation exhibited second-order global accuracy because of the second-order boundary closures.

The representative benchmark and the deterministic first-mode frequency converged to approximately 0.134 Hz, and the steady-state top-displacement amplitude converged to the value 37.22 mm. The fuzzy analysis showed that the peak top displacement widened from a crisp value at $\alpha = 1$ to the interval $[28.06,\ 47.87]$ mm at $\alpha = 0$, expressing that parameter imprecision can substantially enlarge the required response band even in a regular-wave regime.

The dominant contributors to response width were the inertia coefficient C_M and the wave height H, followed by the elastic modulus E. The drag coefficient C_D and damping ratio ξ were comparatively weak contributors in the adopted loading range. The proposed method is therefore suitable for expected preliminary uncertainty-aware serviceability assessment, parameter prioritization, and mechanics-based preprocessing for future SHM, digital-twin, fatigue, and with control-oriented studies of fixed marine support structures. The limited interaction-residual check further indicates that the main-effects ranking is adequate for this moderate benchmark. Before site-specific design use, however, the model should be validated against detailed finite element, experimental, or field-response data.

Author Contributions

All authors contributed equally to the conception, design, data collection, analysis, and writing of this study. All authors have read and agreed to the published version of the manuscript.

Funding

This research was partially funded by INTI International University.

Institutional Review Board Statement

Not applicable.

Informed Consent Statement

Not applicable.

Data Availability Statement

The data used in this study are available from the corresponding author upon reasonable request.

Conflicts of Interest

The authors declare no conflict of interest.

AI Use Statement

The authors declare that no artificial intelligence (AI) tools were used in the preparation of this manuscript.

References

[1] Amiri, N., Shaterabadi, M., Reza Kashyzadeh, K., et al., 2021. A Comprehensive Review on Design, Monitoring, and Failure in Fixed Offshore Platforms. Journal of Marine Science and Engineering. 9(12), 1349. DOI: https://doi.org/10.3390/jmse9121349

[2] Amaechi, C.V., Reda, A., Butler, H.O., et al., 2022. Review on Fixed and Floating Offshore Structures. Part I: Types of Platforms with Some Applications. Journal of Marine Science and Engineering. 10(8), 1074. DOI: https://doi.org/10.3390/jmse10081074

[3] Amaechi, C.V., Reda, A., Butler, H.O., et al., 2022. Review on Fixed and Floating Offshore Structures. Part II: Sustainable Design Approaches and Project Management. Journal of Marine Science and Engineering. 10(7), 973. DOI: https://doi.org/10.3390/jmse10070973

[4] Ramezani, M., Choe, D.-E., Heydarpour, K., et al., 2023. Uncertainty Models for the Structural Design of Floating Offshore Wind Turbines: A Review. Renewable and Sustainable Energy Reviews. 185, 113610. DOI: https://doi.org/10.1016/j.rser.2023.113610

[5] Amouzadrad, P., Mohapatra, S.C., Guedes Soares, C., 2025. Review on Sensitivity and Uncertainty Analysis of Hydrodynamic and Hydroelastic Responses of Floating Offshore Structures. Journal of Marine Science and Engineering. 13(6), 1015. DOI: https://doi.org/10.3390/jmse13061015

[6] Zadeh, L.A., 1965. Fuzzy Sets. Information and Control. 8(3), 338–353. DOI: https://doi.org/10.1016/S0019-9958(65)90241-X

[7] Hanss, M., 2005. Applied Fuzzy Arithmetic: An Introduction with Engineering Applications. Springer-Verlag: Berlin/Heidelberg, Germany. DOI: https://doi.org/10.1007/b138914

[8] Morison, J.R., Johnson, J.W., Schaaf, S.A., 1950. The Force Exerted by Surface Waves on Piles. Journal of Petroleum Technology. 2(5), 149–154. DOI: https://doi.org/10.2118/950149-G

[9] Leng, D., Zhu, Z., Xu, K., et al., 2021. Vibration Control of Jacket Offshore Platform through Magnetorheological Elastomer (MRE) Based Isolation System. Applied Ocean Research. 114, 102779. DOI: https://doi.org/10.1016/j.apor.2021.102779

[10] Leng, D., Zhu, Z., Xu, K., et al., 2022. Neuro Fuzzy Logic Control of Magnetorheological Elastomer Isolation System for Vibration Mitigation of Offshore Jacket Platforms. Ocean Engineering. 253, 111293. DOI: https://doi.org/10.1016/j.oceaneng.2022.111293

[11] Sardar, R., Chakraborty, S., 2022. Wave Vibration Control of Jacket Platform by Tuned Liquid Dampers. Ocean Engineering. 247, 110721. DOI: https://doi.org/10.1016/j.oceaneng.2022.110721

[12] Sardar, R., Chakraborty, S., 2023. Wave Induced Vibration Control of Offshore Jacket Platform by Tuned Liquid Damper with Floating Base. Ocean Engineering. 273, 113948. DOI: https://doi.org/10.1016/j.oceaneng.2023.113948

[13] Lin, H., Luan, H.C., Uzdin, A.M., et al., 2024. A CFD-FEA Coupled Model for Simulating Dynamic Response of Offshore Jacket Platform under Earthquake Considering Wind, Wave, Current and Aftershock Loads. Ocean Engineering. 300, 117481. DOI: https://doi.org/10.1016/j.oceaneng.2024.117481

[14] Liu, S., Li, H., Zhang, J., et al., 2024. Shaking Table Test and Numerical Simulation of Jacket Offshore Platform Considering Soil-Water-Structure Interaction. Ocean Engineering. 313, 119542. DOI: https://doi.org/10.1016/j.oceaneng.2024.119542

[15] Sarkar, N., Konar, T., Ghosh, A.D., 2025. Passive Vibration Control Techniques for Offshore Structures under Different Environmental Loading: A Review. Ocean Engineering. 320, 120296. DOI: https://doi.org/10.1016/j.oceaneng.2025.120296

[16] Cai, Z., Zhang, B.-L., Han, Q.-L., et al., 2025. Sampled-Data Fuzzy Modeling and Control for Offshore Structures Subject to Parametric Perturbations and Wave Loads. Ocean Engineering. 326, 120908. DOI: https://doi.org/10.1016/j.oceaneng.2025.120908

[17] Liu, S., Zhang, J., Yin, X., et al., 2025. A Hybrid VMD-IGA-LSTM Model for Dynamic Response Prediction of Jacket Offshore Platform. Ocean Engineering. 328, 121110. DOI: https://doi.org/10.1016/j.oceaneng.2025.121110

[18] Bodaghi, F., Aghakouchak, A.A., 2025. Probabilistic Seismic Analysis of Jacket-Type Offshore Platforms: A Study on Structural and Non-Structural Limit States and Failure Probabilities. Ocean Engineering. 323, 120555. DOI: https://doi.org/10.1016/j.oceaneng.2025.120555

[19] Jiang, K., Li, H., Lv, G., et al., 2025. Vibration Control of Deepwater Offshore Platform Using Viscous Dampers under Wind, Wave, and Earthquake. Journal of Marine Science and Engineering. 13(7), 1197. DOI: https://doi.org/10.3390/jmse13071197

[20] Ma, R., Bi, K., Zuo, H., et al., 2023. Inerter-based damping isolation system for vibration control of offshore platforms subjected to ground motions. Ocean Engineering. 280, 114726. DOI: https://doi.org/10.1016/j.oceaneng.2023.114726

[21] Patil, K.C., Jangid, R.S., 2005. Passive control of offshore jacket platforms. Ocean Engineering. 32(16), 1933–1949. DOI: https://doi.org/10.1016/j.oceaneng.2005.01.002

[22] Gavgani, S.A.M., Hosseini Lavassani, S.H., 2024. Vibration Mitigation of Offshore Structures Subjected to Wave and Wind Loads Using Optimum Semi-Active Tuned Mass Damper Inerter (SATMDI). Ocean Engineering. 297, 117110. DOI: https://doi.org/10.1016/j.oceaneng.2024.117110

[23] Hu, Z., Xiong, T., Gao, X., et al., 2025. Study on the Structural Vibration Control of a 10 MW Offshore Wind Turbine with a Jacket Foundation Under Combined Wind, Wave, and Seismic Loads. Journal of Marine Science and Engineering. 13(11), 2112. DOI: https://doi.org/10.3390/jmse13112112

[24] Sardar, R., Chakraborty, S., 2025. Vibration Control of Offshore Structures Using Liquid Dampers: A Review. Ocean Engineering. 329, 121078. DOI: https://doi.org/10.1016/j.oceaneng.2025.121078

[25] Yang, Y., Liang, F., Zhu, Q., et al., 2024. An Overview on Structural Health Monitoring and Fault Diagnosis of Offshore Wind Turbine Support Structures. Journal of Marine Science and Engineering. 12(3), 377. DOI: https://doi.org/10.3390/jmse12030377

[26] Wang, M., Incecik, A., Tian, Z., et al., 2024. Struc-

tural Health Monitoring on Offshore Jacket Platforms Using a Novel Ensemble Deep Learning Model. Ocean Engineering. 301, 117510. DOI: https://doi.org/10.1016/j.oceaneng.2024.117510

[27] Pastor-Sanchez, A., Garcia-Espinosa, J., Di Capua, D., et al., 2025. Real-Time Digital Twin for Structural Health Monitoring of Floating Offshore Wind Turbines. Journal of Marine Science and Engineering. 13(10), 1953. DOI: https://doi.org/10.3390/jmse13101953

[28] Ye, H., Jiang, C., Zu, F., et al., 2022. Design of a Structural Health Monitoring System and Performance Evaluation for a Jacket Offshore Platform in East China Sea. Applied Sciences. 12(23), 12021. DOI: https://doi.org/10.3390/app122312021

[29] Dong, Y., Garbatov, Y., Guedes Soares, C., 2022. Review on Uncertainties in Fatigue Loads and Fatigue Life of Ships and Offshore Structures. Ocean Engineering. 264, 112514. DOI: https://doi.org/10.1016/j.oceaneng.2022.112514

[30] Martínez, R.D.Á.B., Álvarez-Arellano, J.A., El Hamzaoui, Y., 2025. Assessment of Structural Integrity through On-Site Decision-Making Analysis for a Jacket-Type Offshore Platform. Applied Sciences. 15(7), 3418. DOI: https://doi.org/10.3390/app15073418

[31] Cao, D., Jiang, X., Wu, H., et al., 2025. Fatigue Analysis of Offshore Steel Structures: A Systematic Review. Structures. 79, 109489. DOI: https://doi.org/10.1016/j.istruc.2025.109489